catalysts

MDPI

Article

Catalytic Effect of CaO and ZSM-5 on Microalgae Pyrolysis Under Reverse Chemical Looping Pyrolysis Conditions

Weiwei Zhang [1,*], Weiwei Li [1], Xiaozhen Kang [1] and Yongzhuo Liu [2,*]

[1] College of Applied Chemical Engineering, Lanzhou Petrochemical University of Vocational Technology, Lanzhou 730060, China; liweiwei@lzpuvt.edu.cn (W.L.); kangxiaozhen@lzpuvt.edu.cn (X.K.)
[2] Laboratory of Green & Smart Chemical Engineering in Universities of Shandong, College of Chemical Engineering, Qingdao University of Science and Technology, Qingdao 266042, China
* Correspondence: qust654321@163.com (W.Z.); yzliu@qust.edu.cn (Y.L.)

Abstract

Integrating catalytic function with oxygen-carrying capability into bi-functional materials represents a promising strategy for reverse chemical looping pyrolysis (RCLPy), which utilizes a reduced metal oxide to improve the bio-oil quality through in situ hydrogen donation and deoxygenation. In this study, a systematic evaluation of two typical catalysts (CaO and ZSM-5) was conducted for the pyrolysis of microalgae *Nannochloropsis* sp. under RCLPy conditions. First, the effect of each catalyst on the pyrolysis behavior of microalgae was analyzed by Gaussian fitting of derivative thermogravimetric (DTG) curves. Second, gases evolved during thermogravimetric analysis (TGA) were monitored in real time using Fourier-transform infrared spectroscopy (FTIR) for detecting CO, CO_2, H_2O, and functional groups (e.g., C–C, C=C, C=O), and mass spectrometry (MS) for tracking nitrogen-containing compounds. Third, the composition of bio-oils produced under RCLPy conditions was examined by Gas Chromatography–Mass Spectrometer (GC–MS) analysis. The results demonstrate that the catalyst enhances the bio-oil quality by elevating the content of aromatics up to 41.9 area% and that of aliphatic hydrocarbons to 19.1 area%, respectively, while reducing the content of nitrogen-containing compounds to 3.8 area%. However, the elimination pathway of oxygen and nitrogen elements involves different mechanisms. These findings provide valuable guidance for the design of bifunctional oxygen carriers aimed at enhancing the quality of bio-oil derived from microalgae pyrolysis.

Keywords: catalytic pyrolysis; nitrogen migration; microalgae biomass; reverse chemical looping pyrolysis

Check for updates

Academic Editor: Changzhi Li

Received: 23 December 2025
Revised: 20 January 2026
Accepted: 28 January 2026
Published: 29 January 2026

Copyright: © 2026 by the authors. Licensee MDPI, Basel, Switzerland. This article is an open access article distributed under the terms and conditions of the Creative Commons Attribution (CC BY) license.

1. Introduction

Microalgae, as promising feedstocks for third-generation biofuels, have garnered significant attention, owing to their rapid growth rates, high CO_2 fixation efficiency, and the absence of competition with arable land resources [1]. Unlike lignocellulosic biomass, microalgae primarily consist of carbohydrates, proteins, and lipids, eliminating the need for complex pretreatment processes prior to conversion [2]. The pyrolysis process offers a direct route to convert these constituents into bio-oils, syngas, and biochar, demonstrating considerable potential for energy production and carbon emission mitigation [3,4]. However, microalgae-derived bio-oil typically suffers from high oxygen and nitrogen content, resulting in undesirable properties such as low calorific value (15–29 MJ/kg), high water content (15–50 wt.%), low pH (2.0–3.8), poor chemical stability, and the potential release of

NO_x pollutants upon combustion [5–7]. These limitations have driven the development of catalytic pyrolysis, primarily via in situ and ex situ approaches, to upgrade bio-oil quality [8]. In situ catalytic pyrolysis, where biomass is mixed directly with catalysts, offers operational simplicity, but faces challenges in catalyst recovery and regeneration [9–11]. Conversely, ex situ catalytic pyrolysis spatially separates pyrolysis and catalytic upgrading, which mitigates catalyst deactivation and extends catalyst life at the expense of increased system complexity and equipment demands [12].

Recently, Liu et al. [13] proposed a novel process, termed reverse chemical looping pyrolysis (RCLPy). This approach utilizes a reduced oxygen carrier to transfer oxygen from the biomass, thereby gasifying pyrolytic semi-char in a separate stage. By reversing the oxygen transfer direction, the reduced oxygen carrier not only oxidizes bio-oil intermediates to reduce the oxygen content but also generates hydrogen via reactions with small-molecule oxygenates [14,15]. Consequently, RCLPy is anticipated to minimize the loss of carbon and hydrogen generated in the form of CO_2 and H_2O. Integrating chemical looping with conventional catalytic pyrolysis could substantially alleviate challenges related to catalyst regeneration and process complexity, presenting a promising strategy for microalgae pyrolysis [16]. To the best of our knowledge, the catalytic performance of conventional pyrolysis catalysts under RCLPy conditions—particularly as influenced by key operational parameters such as temperature and catalyst-to-feedstock ratio—remains scarcely explored. Thus, screening suitable catalytic components for RCLPy is warranted.

Among reported catalysts for biomass pyrolysis, zeolites ZSM-5 and CaO are frequently used for microalgae upgrading. ZSM-5 features a unique cross three-dimensional pore structure and tunable acidity [5,6], whereas CaO exhibits strong deoxygenation and decarboxylation capabilities [17], along with CO_2 absorption properties [18,19]. Razzak et al. [20] noted that catalysts such as Cu/HZSM-5, Ni-Mg/ZSM-5, CaO, and Ce improve the bio-oil quality and yield by reducing nitrogenous and oxygenated compounds while promoting the formation of high-value aromatic hydrocarbons. Guo et al. [21] further indicated that CaO derived from the hydration–calcination cycle significantly lowered oxygen content in bio-oil from *Nannochloropsis* sp. pyrolysis, markedly reducing its moisture content and viscosity. In summary, zeolites and CaO are established as efficient catalysts for both in situ and ex situ biomass pyrolysis and show considerable promise for microalgae pyrolysis. Nevertheless, studies focusing on the simultaneous deoxygenation and denitrogenation of microalgae-derived bio-oil remain limited [22–24]. Moreover, the catalytic behavior of zeolites and CaO under RCLPy conditions, especially regarding nitrogen migration—a critical issue given the high protein content of microalgae, requires deeper investigation.

In this study, the pyrolysis characteristics of *Nannochloropsis* sp., a typical microalga, were investigated using CaO and ZSM-5 as catalysts. The aim is to develop a comprehensive understanding of the influence of these typical catalysts on microalgae pyrolysis and nitrogen migration under RCLPy conditions. By analyzing product distribution, gas composition, and nitrogen transformation pathways, this work seeks to provide fundamental insights for designing bifunctional oxygen carriers tailored to the microalgae RCLPy process, thereby contributing to the production of high-quality bio-oil from microalgal biomass.

2. Results and Discussion

2.1. TG-DTG Analysis of Microalgae Catalytic Pyrolysis

The mass loss and mass loss rate of microalgae pyrolysis from ambient temperature to 800 °C are shown in Figure 1. As illustrated in Figure 1a, the pyrolysis process can be divided into three stages: dehydration (below 150 °C), main cracking (150–600 °C), and deep decomposition (above 600 °C). The mass loss profiles differ markedly between

non-catalytic and catalytic runs. Compared with the blank experiment under the same thermal conditions, ZSM-5 leads to greater mass loss, reaching 41 wt.% at the end of pyrolysis, indicating its catalytic promotion of microalgae decomposition. In contrast, CaO shows lower mass loss than the other two cases before 710 °C, but ultimately attains the highest total mass loss of 42 wt.%. This behavior is primarily attributed to ketonization reactions between CaO and pyrolysis intermediates [25]. Furthermore, the CaO-derived intermediates begin to decompose into CaO and CO_2 above 600 °C, as evidenced by the subsequent FTIR analysis.

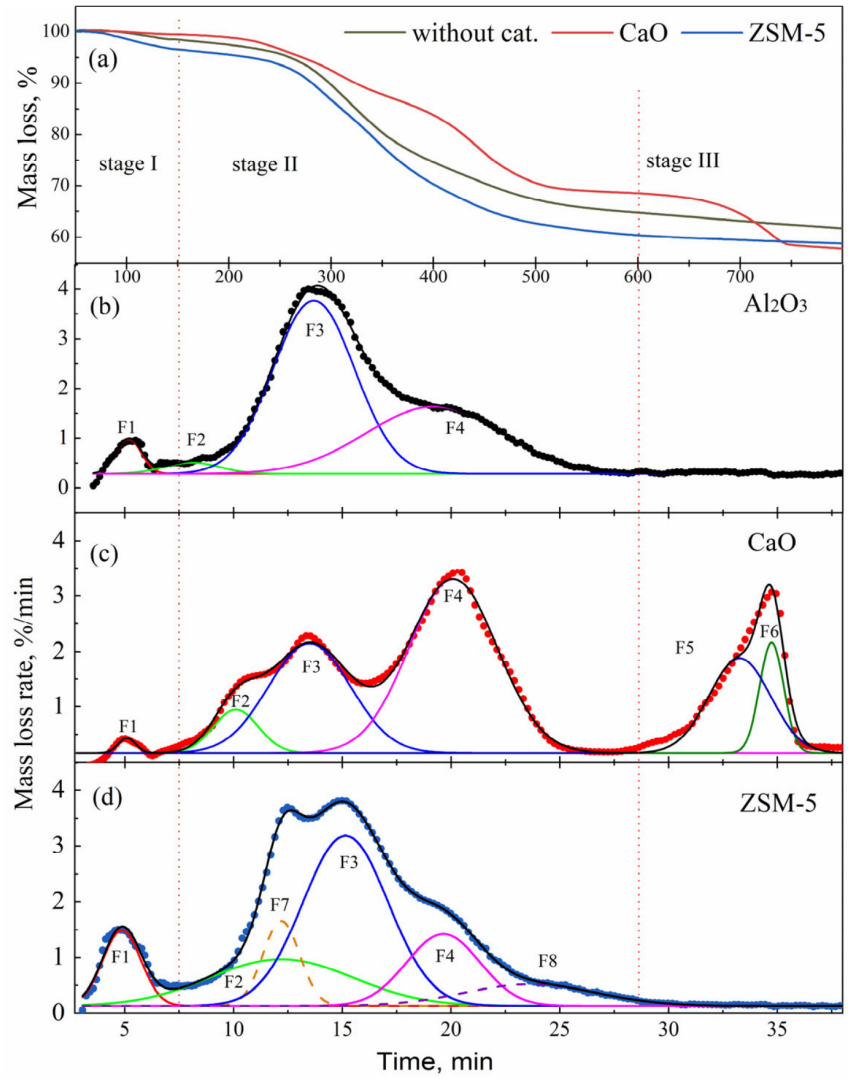


Figure 1. TG and DTG curves of the mixture of microalgae with and without catalysts. (**a**) Mass loss as a function of temperature; (**b**–**d**) mass loss curve as a function of time and their fitting peaks using a Gaussian function(scattered dots: original data; red line: fitting peak F1; green line: fitting peak F2, blue line: fitting peak F3; magenta line: fitting peak F4; navy line: fitting peak F5; olive line: fitting peak F6; wine line: fitting peak F7; violet line: fitting peak F8).

The influence of the two catalysts on the thermal decomposition of microalgae is clearly reflected in the derivative DTG curves presented in Figure 1b–d. Each DTG profile was fitted using a multi-Gaussian function comprising several overlapping sub-reactions, with a correlation coefficient exceeding 0.997 [14]. Based on previous reports [26], Peak F1–F4 can be tentatively assigned to the dehydration of the mixture and the thermal degradation of carbohydrates, proteins, and lipids, respectively. Compared with the blank experiment, CaO shifts the carbohydrates pyrolysis peak (F2) to higher temperatures, reduces the

proteins-derived peak (F3), and increases the lipid-related peak (F4). This suggests that CaO preferentially interacts with protein pyrolysis products, with subsequent release of volatiles via decomposition. Two additional mass loss rate peaks (F5 and F6) are observed, corresponding to the thermal decomposition of CaO-derived intermediates, i.e., calcium carboxylate and $CaCO_3$, which formed via the ketonization reaction and CO_2 adsorption reaction, respectively [27]. In the case of the ZSM-5 catalyst, more complex reactions occur. In addition to the characteristic peaks (F2–F4) for the three principal microalgae constituents, two extra fitting peaks appear at approximately 250 °C (F7) and 505 °C (F8). Peak F7 is associated with protein pyrolysis, while Peak F8 likely reflects the deep catalytic cracking of microalgae constituents over ZSM-5. Notably, the protein-related peak (F3) is significantly enhanced, though its position shifts toward higher temperatures.

2.2. FTIR Analysis of Catalytic Pyrolysis Products

To investigate the composition of products during catalytic pyrolysis, evolved gases from TGA were analyzed in real time by FTIR. The transfer line between the TG unit and the FTIR spectrometer was maintained at 200 °C, allowing both pyrolysis gases and organic compounds containing fewer than 11 carbon atoms to enter the gas cell and be effectively detected [14]. According to the Lambert–Beer law, absorbance is directly proportional to the concentration of absorbing species, establishing a linear relationship. Therefore, the relative absorbance of functional groups (C–C, C=C, and C=O) and specific species (CO_2, CO, and H_2O) can serve as an indicator of their relative concentrations. Characteristic absorption bands for C–C, C=C, and C=O groups are located near 2900 cm^{-1}, 1650 cm^{-1}, and 1750 cm^{-1}, corresponding to alkanes, olefins, and low-molecular-weight carbonyl compounds (e.g., acids, ketones, and esters), respectively [28]. Additionally, distinct absorbance peaks for CO_2, CO, and H_2O appear at approximately 2340 cm^{-1}, 2180 cm^{-1}, and 3600 cm^{-1}, respectively.

The effect of temperature and catalysts on three typical functional groups (C–C, C=C, and C=O) is illustrated in Figure 2. As for C–C functional groups, two absorbance peaks appear at 350 °C and 483 °C in the non-catalytic run. Comparison with Figure 1b suggests that these peaks are primarily attributed to the pyrolysis of proteins and lipids, respectively. With CaO as the catalyst, two absorbance peaks emerge at 268 °C and 483 °C. By reference to Figure 1c, the former peak is likely associated with the cracking of carbohydrates, while the latter corresponds to lipid decomposition. Notably, the intensity of the latter peak is approximately four times higher than that in the non-catalytic case, suggesting that CaO markedly promotes C–C bond formation. When ZSM-5 is used, the maximum absorbance occurs at 442 °C, higher than that without a catalyst, suggesting that ZSM-5 also enhances alkane generation but shifts the reaction to a higher temperature.

For C=C functional groups, the strongest absorbance peak in the absence of catalysts appears at 345 °C, within the temperature range related to protein decomposition, as shown in Figure 1b. In the presence of either catalyst, the intensity of the absorbance peaks increases substantially. Additional peaks around 442 °C are observed for both catalysts, corresponding to lipid pyrolysis, and reflecting catalytic decarboxylation and dehydrogenation. Additionally, a minor absorbance peak at 594 °C implies that CaO facilitates deep cracking reactions to yield more alkanes at higher temperatures.

Regarding C=O groups, the maximum absorbance peak in the non-catalytic experiment occurs at 326 °C and gradually decreases with rising temperature, indicating that carbonyl compounds are mainly generated from protein cracking. In the presence of CaO, two distinct absorbance peaks at 274 °C and 446 °C are observed, which fall within the decomposition ranges of carbohydrates and lipids, respectively. In the case of ZSM-5, the absorbance above 200 °C is the lowest among all conditions, underscoring its superior

deoxygenation capability. A distinct peak at 130 °C indicates that ZSM-5 also catalyzes carbohydrate cracking at relatively low temperatures.

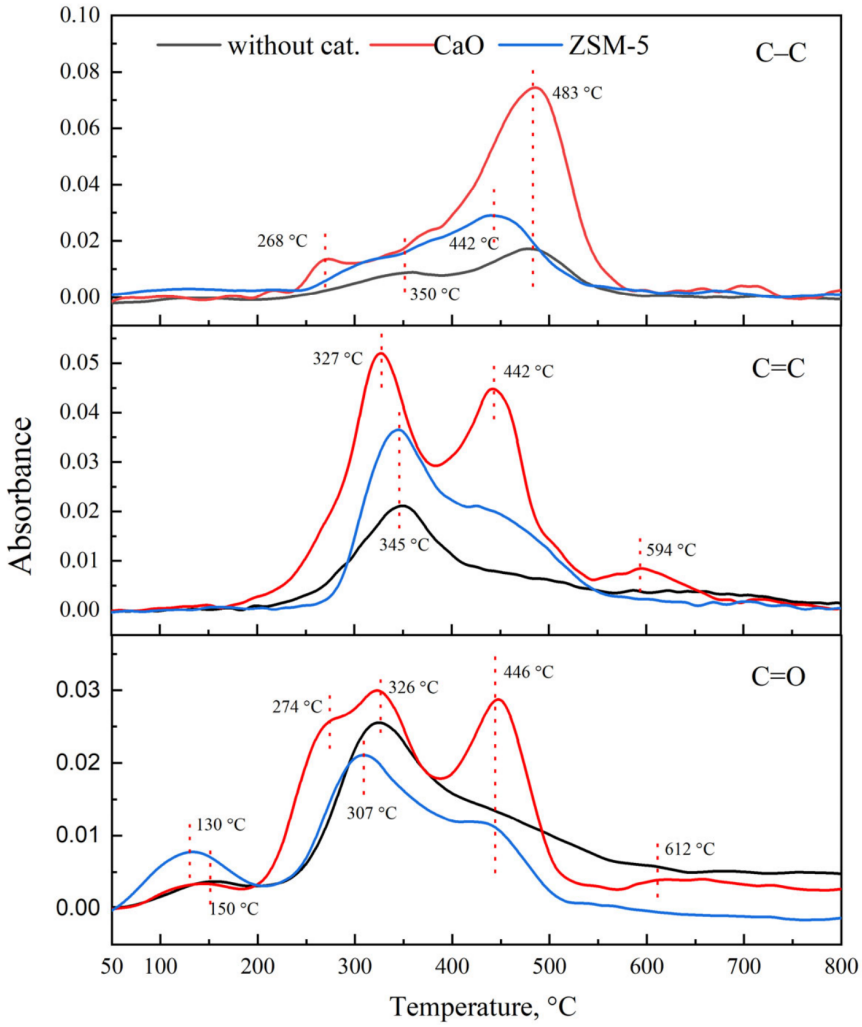


Figure 2. Variation curve of typical function groups as a function of temperature.

The effect of temperature and catalysts on the evolution of typical gaseous products (CO_2, CO, and H_2O) is illustrated in Figure 3. As for CO_2, the lowest adsorption peak observed with CaO at 600 °C results from its chemical adsorption by CaO. However, when the temperature exceeds 600 °C, the adsorbed CO_2 begins to release due to the thermodynamic facilitation of $CaCO_3$ calcination at higher temperatures. Therefore, the catalytic role of CaO involves a cyclic process of carbonization at low temperature and regeneration at high temperature. Previous studies have shown that CaO catalyzes the ketonization of oxygen-containing pyrolysis intermediates, generating ketones, CO_2, and H_2O, while simultaneously adsorbing CO_2 from the pyrolysis stream [29]. In contrast, the prominent CO_2 absorbance peak at 338 °C with ZSM-5 reflects enhanced deoxygenation of pyrolysis vapors, consistent with the C=O absorbance trends noted earlier. Concerning CO, detectable absorbance peaks appear only when CaO is employed as the catalyst, likely resulting from the reaction between $CaCO_3$ and the semi-char produced during the process. The generation of both CO_2 and CO represents effective deoxygenation of bio-oil precursors; however, it also corresponds to carbon loss from the biomass that does not contribute to the liquid product.

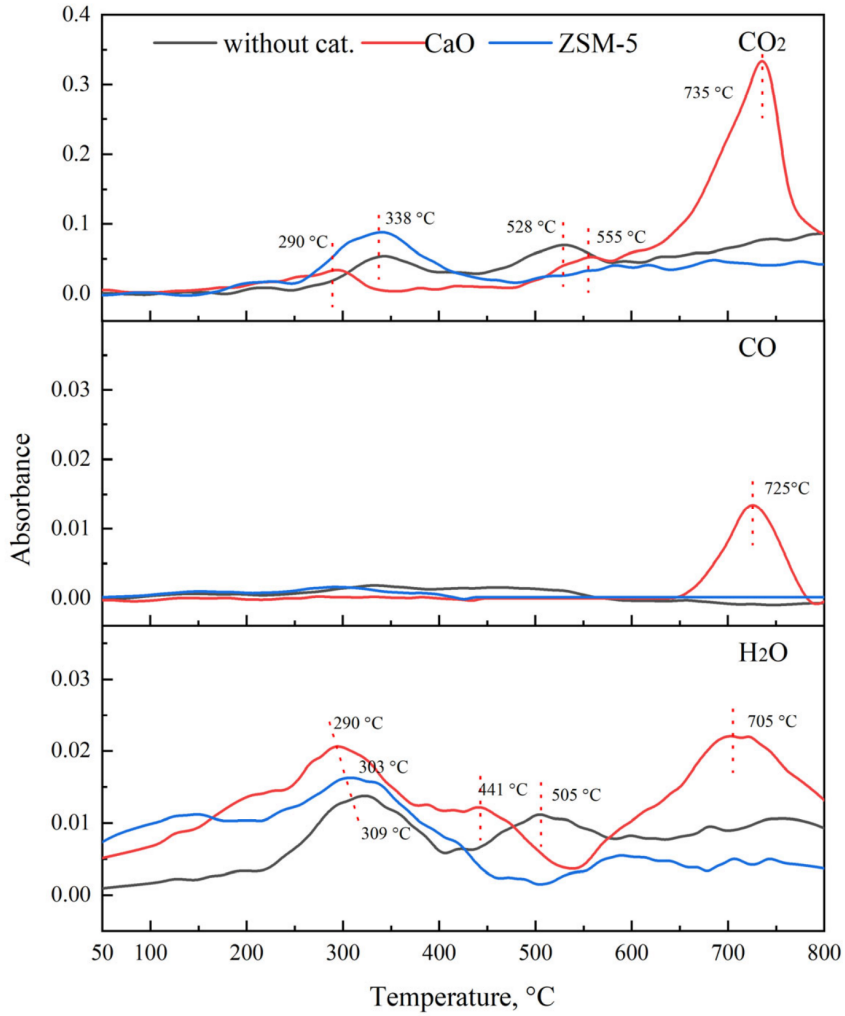


Figure 3. Variation curve of typical gaseous products as a function of temperature.

As for H_2O, absorbance peaks below 200 °C are ascribed to sample drying and partial cracking of carbohydrates, while those near 300 °C are linked with protein decomposition. Notably, the peak temperatures in catalytic runs are lower than those in non-catalytic pyrolysis. In the lipid decomposition zones, neither CaO nor ZSM-5 produced distinct absorbance peaks of H_2O. An additional absorbance peak at 705 °C in the presence of CaO probably stems from the deep dehydration of the semi-char under the catalysis of CaO. H_2O evolution represents another deoxygenation pathway for bio-oil, yet it also constitutes a major route of hydrogen loss from the biomass. Compared with traditional catalytic pyrolysis, RCLPy uses a reduced metal oxide to remove oxygen from bio-oil intermediates while supplying in situ hydrogen for upgrading. The H_2O derived from low-temperature catalytic pyrolysis could therefore serve as an efficient hydrogen source in an integrated RCLPy system, where the oxygen-carrying functionality is combined with the catalytic functions described above.

2.3. MS Analysis of Nitrogen-Containing Gaseous Products

To investigate the release behavior of nitrogen-containing gaseous products, evolved gases from TGA were monitored in real time using MS. Four typical nitrogen-containing gaseous products, NH_3, HCN, HCNO, and NO, were tracked. As shown in Figure 4, a distinct NH_3-release peak appears near 300 °C in all three cases, primarily attributed to protein cracking. In the presence of CaO, however, a pronounced peak at 430 °C with substantially higher intensity is observed, indicating a strong catalytic promotion on NH_3

release, which is consistent with previous reports [30]. HCN is primarily formed through the decomposition of nitrile-N and heterocyclic-N compounds. Given the low abundance of heterocyclic-N structures in microalgae, nitrile-N serves as the predominant source of HCN [31]. Nitrile-N originates from the hydrolysis of amides, which are produced by the reaction between lipid-derived carboxylic acids and NH_3 [32]. Furthermore, CaO can promote ring-opening reactions and enhance the conversion of amine-N to intermediate nitrile-N [33]. Amides can also thermally decompose into HCNO, which subsequently cracks into HCN. Consequently, the temperature of the maximum release peak increases in the order: NH_3 < HCNO < HCN. The highest HCNO release observed with CaO is closely correlated with the formation of amides, as evidenced by the pronounced NH_3 peak at 430 °C. Compared with the two distinct HCN peaks at 290 °C and 486 °C in the absence of catalysts, both CaO and ZSM-5 effectively suppress the formation of HCN. This phenomenon is probably associated with their reactions with HCN or their suppression effect on the formation of nitrile-N. Regarding NO, similar evolution profiles are observed for all three conditions, presumably attributed to the decomposition of HCNO and oxidation of other N-containing species.

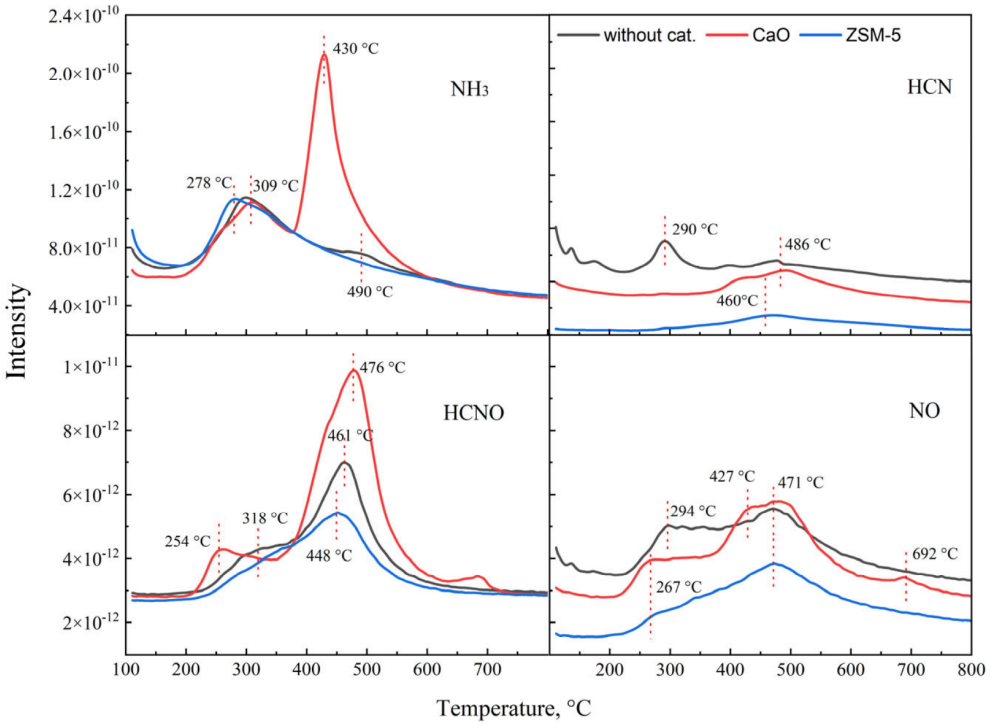


Figure 4. Variation curve of nitrogen-containing products as a function of temperature.

2.4. Gas–Liquid-Solid Phase Distribution at Different Pyrolysis Temperatures

Based on the TG analysis results, two typical temperatures for the microalgae RCLPy process [14], 450 °C and 600 °C, were selected to examine pyrolysis behavior under non-catalytic, CaO catalytic, and ZSM-5 catalytic conditions. Product distribution among gas, liquid, and solid phases was determined using a tubular reactor system. The solid-phase yield was calculated based on the weight difference of the reactor before and after pyrolysis. The liquid-phase yield was determined by weighing the condensation traps, and the gas-phase yield was obtained by mass balance. All yields are expressed as mass percentages relative to the initial biomass. As shown in Figure 5, the liquid-phase yield increases and the solid-phase yield decreases as the temperature increases from 450 °C to 600 °C under all three conditions. Compared with the control at the same temperature, ZSM-5 produces a higher liquid-phase yield, reaching a maximum liquid-phase yield of 69% at

600 °C. In contrast, CaO leads to a lower liquid-phase yield and a correspondingly higher share of solid or gaseous products, with the highest solid-phase yield of 41% at 450 °C and the highest gaseous phase of 21% at 600 °C. At 450 °C, CaO reacts with CO_2 and liquid intermediates, leading to an increase in the solid phase through carbonation and related reactions. When the temperature rises to 600 °C, CaO facilitates further cracking of pyrolysis products, enhancing gas formation. These trends align well with the TG-FTIR observations discussed earlier.

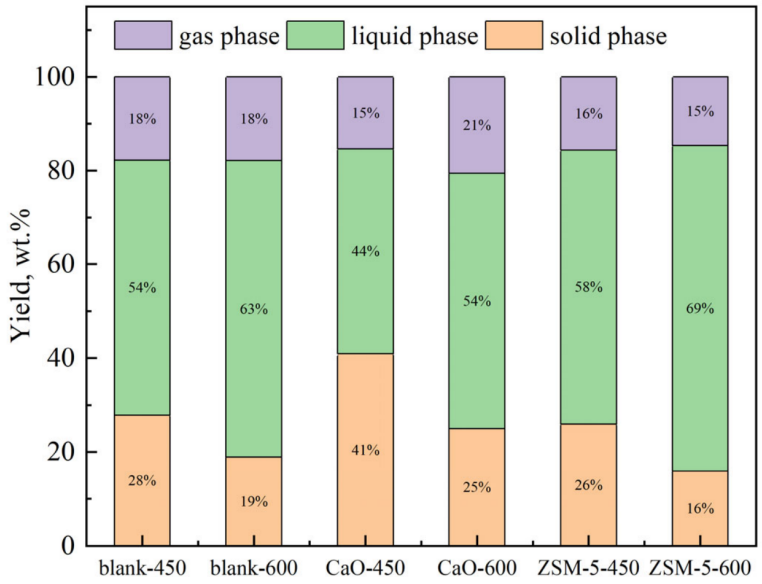


Figure 5. Gas–liquid-solid phase distribution at different pyrolysis temperatures without catalysts and in the presence of CaO and ZSM-5.

2.5. GC-MS Analysis of Pyrolysis Liquid Products

The collected bio-oil was dehydrated and subsequently characterized using GC-MS. Due to the complexity of the mixture and the lack of commercial standards, GC-MS was unable to provide absolute quantitative data for the individual compounds. Nevertheless, the chromatographic peak area percentage for each compound can be reasonably assumed to correlate linearly with its relative concentration in the bio-oil. Therefore, the peak-area percentage was utilized to represent the relative abundance of compounds under varying conditions. To more effectively illustrate the influence of catalysts on major functional groups, the identified compounds were categorized into five groups according to previous studies [5,6]: aromatics, phenols, aliphatic hydrocarbons (including alkanes and olefins), oxygenated compounds (including alcohol, carboxylic acid, ketone, and ester), and nitrogen-containing compounds (such as nitrile-N and heterocyclic-N). Collectively, the peak areas of these five groups accounted for over 97% of the total peak area.

The composition distribution of pyrolysis liquids obtained at two typical temperatures under non-catalytic, CaO-catalytic, and ZSM-5 catalytic conditions is summarized in Figure 6 and Tables S1–S6. Temperature significantly influenced the bio-oil composition: higher temperature increases the relative content of aromatics, phenols, and aliphatic hydrocarbons, while decreasing those of oxygenated and nitrogen-containing compounds. In the absence of a catalyst, the relative content of aromatics rises from 3.5 area% to 12.8 area%, and aliphatic hydrocarbons from 13.1 area% to 21.6 area%, whereas oxygenated compounds markedly decrease from 38.9 area% to 22.4 area% as the temperature rises from 450 °C to 600 °C. This shift is mainly attributed to enhanced cracking of oxygenated compounds, primarily consisting of carboxylic acids, at higher temperatures, which promotes the formation of aromatics and olefins. However, the relative content of N-containing compounds

remains consistently high (>40 area%), with pentadecanenitrile alone contributing up to 19.6 area%. This suggests that elevated temperature alone has a limited effect on the denitrification of nitrile-derived nitrogen.

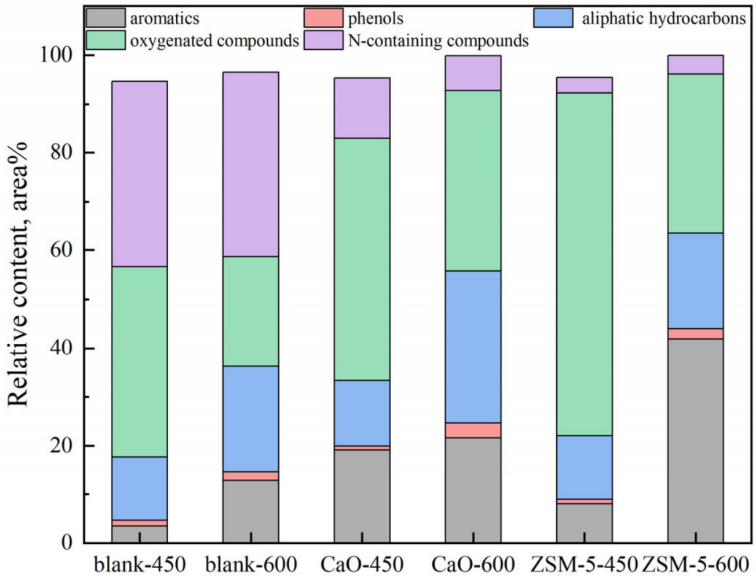


Figure 6. Composition distribution of pyrolysis liquid products at 450 °C and 600 °C without catalysts and in the presence of CaO and ZSM-5 catalyst.

At the same temperature, both catalysts greatly change the relative contents of the five groups. With CaO at 600 °C, the relative aromatic content increases from 12.8 area% (non-catalytic) to 21.6 area%, and aliphatic hydrocarbons from 21.6 area% to 31.1 area%, while nitrogen-containing compounds decrease from 37.9 area% to 7.1 area%. These changes are attributed mainly to decarboxylation and denitrification reactions catalyzed by CaO. Decarboxylation generates aliphatic hydrocarbons, as evidenced by the elimination of n-hexadecanoic acid. Denitrification reaction refers to the nitrogen removal of nitrile compounds, with pentadecanenitrile content decreasing to zero. The CaNx formed from the reaction between CaO and nitrile further hydrolyzes, resulting in the release of nitrogen in the form of NH_3, which is consistent with the MS observations of nitrogen-containing gaseous products. The corresponding liquid products likely include ketones, given the appearance of 15.5 area% cyclopentadecanone alongside the disappearance of oleanitrile and pentadecanenitrile. ZSM-5, with its unique three-dimensional pore structure and adjustable acidity, is an effective catalyst for the aromatization of light olefins [34]. This leads to high aromatic yield up to 41.9 area% and aliphatic hydrocarbons of up to 19.1 area%. Moreover, the strong Brønsted acidic sites of ZSM-5 promote C-N bond cleavage through reactions such as deamination, thereby facilitating the release of nitrogen in gaseous forms like NH_3 and HCN or char phase rather than retention in liquid-phase products [8]. Consequently, the relative content of N-containing compounds in the liquid-phase products is only 3.8 area%. Nevertheless, this result appears inconsistent with the MS data mentioned above, possibly because N_2, which has the same molecular weight as CO, was not distinguished in the MS analysis. An alternative explanation is the retention of nitrogen in the pyrolysis char. However, the exact mechanism remains unclear due to the complexity of surface reactions and potential side processes, warranting further investigation.

Although the overall proportion of oxygenated compounds increases under the catalytic conditions, the oxygenated species are converted from undesirable carboxylic acid to stable ketones and alcohols, which demonstrates the deoxygenation ability of both catalysts. The distribution of oxygenated compounds in pyrolysis liquid products under non-catalytic,

CaO-catalytic, and ZSM-5-catalytic conditions is depicted in Figure 7 and Table S7. Compared with the non-catalytic case, most oxygenated compounds are converted into ketones in the presence of CaO, accompanied by the near-complete disappearance of carboxylic acids. This transformation proceeds mainly through two pathways: First, CaO catalyzes the ketonization reaction, which involves the reaction between two carboxylic acids with α-hydrogen atoms. Generally, it refers to one long-chain linear carboxylic acid and one short-chain carboxylic acid, such as acetic acid and propionic acid. The typical ketone products include 2-heptadecanone and 3-octadecanone. Secondly, as discussed above, CaO can react with nitriles to further generate the ketones. As for the ZSM-5 catalyst, the relative content of oxygenated compounds reaches 70.2 area% at 450 °C, dominated by hexadecenoic acid, Z-11 (10.5 area%) and n-hexadecanoic acid (24.9 area%). Although a higher temperature can promote the further cracking of these oxygenated compounds, with the relative content decreasing to 32.7 area% at 600 °C, it remains higher than that observed without a catalyst. Notably, the relative content of alcohols and esters increases significantly. The generation of alcohols is likely promoted by hydration reactions over the Brønsted acid sites of ZSM-5 [35,36].

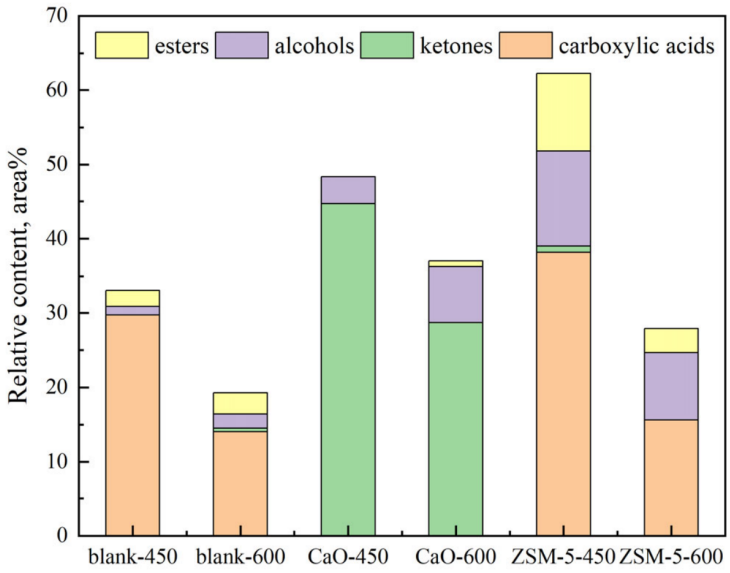


Figure 7. Composition distribution of oxygenated compounds in pyrolysis liquid products at 450 °C and 600 °C without catalysts and in the presence of CaO and ZSM-5 catalyst.

Integrating the findings from TG-FTIR and TG-MS analyses, it is evident that two catalysts exhibit distinct catalytic behaviors. CaO, a typical alkaline earth metal oxide, effectively reduces the content of both oxygenated compounds and nitrogen-containing compounds via reactions with pyrolysis intermediates. Nevertheless, the subsequent need to decompose the resulting CaO-derived species for catalyst regeneration introduces practical complexity. In contrast, ZSM-5 demonstrates significantly superior performance in aromatization reactions due to its unique three-dimensional pore structure and adjustable acidity. The well-defined pore network not only facilitates efficient mass transfer but also promotes the selective conversion of intermediate products toward desirable products. Moreover, its adjustable acidity allows the catalyst to adapt flexibly to different reaction conditions, enhancing its effectiveness in the catalytic cracking. By leveraging the complementary strengths of both catalysts, their rational combination could offer an efficient and viable strategy for advancing microalgae catalytic pyrolysis. For instance, the reduced oxygen carrier for RCLPy not only possesses excellent deoxygenation performance by providing in situ hydrogen to generate bio-oils with a higher heating value [15] and spe-

cific chemicals [37], but also is expected to solve the catalyst regeneration problem by using the chemical looping concept. The catalytic pyrolysis data obtained under simulated RCLPy conditions in this study thus furnish key insights for the future design of integrated, bifunctional oxygen carriers.

3. Materials and Methods

3.1. Preparation of Experimental Materials

Two representative catalysts, namely the solid base CaO and the solid acid ZSM-5, were employed in this study. Analytical grade CaO (>98% purity) was purchased from Sinopharm Group Chemical Reagent Co., Ltd., Shanghai, China. Prior to use, the CaO was calcined at 800 °C for 2 h under a nitrogen atmosphere. After cooling to room temperature, CaO was ground through a 140-mesh sieve (100 μm), sealed, and stored in a desiccator for subsequent use. Its specific surface areas and pore size were determined to be 2.9 m^2/g by the Brunauer–Emmett–Teller method, and 21.1 nm by the Barret–Joyner–Halenda method, respectively. ZSM-5 (Si/Al = 38:1) was obtained from the catalyst plant of Nankai University, Tianjin, China. Its specific surface areas and pore size were determined to be 407.21 m^2/g (BET method) and 2.43 nm (BJH method), respectively. The amounts of weak acid sites and strong acid sites were measured as 0.037 and 0.041 mmol/g, respectively, using NH_3-temperature-programmed desorption (NH_3-TPD) analysis. Additionally, quartz sand was employed as a non-catalytic control in the experiment to exclude catalytic contributions.

The proximate analysis, ultimate analysis, and chemical composition of the purchased *Nannochloropsis* sp., as reported in our previous work [14], are summarized in Table 1. It is evident that microalgae exhibit a remarkably high volatile matter content, primarily attributed to three key chemical constituents: proteins, lipids, and carbohydrates. Additionally, the content of the oxygen element is 35.44%, which results in the unfavorable characteristics of bio-oils, such as high oxygen contents and increased acidity.

Table 1. Proximate analysis, ultimate analysis, and chemical constituents of *Nannochloropsis* sp. [14].

Item	Composition	Content
Proximate analysis wt.%, ad	Moisture	3.90
	Volatile	82.91
	Ash	6.07
	Fixed carbon	7.12
Ultimate analysis, wt.%, daf	Carbon	50.67
	Hydrogen	7.35
	Nitrogen	6.54
	Oxygen (calculated by difference)	35.44
Chemical constituents, wt.%	Proteins	44
	Lipids	30
	Carbohydrates	21

3.2. Experimental Setup and Methods

The catalytic pyrolysis experiments of microalgae were conducted using a thermogravimetric analyzer (TGA, STA409 PC, Netzsch, Selb, Germany). Specifically, approximately 15 mg of a mixture consisting of catalyst and *Nannochloropsis* sp. with a weight ratio of 1:1, similar to RCLPy, was placed into an alumina crucible. The mixture was then heated from ambient temperature to 800 °C under an inert atmosphere at a heating rate of 20 °C/min. The flow rate of inert gas was maintained at 100 mL/min. The emitted gas from TGA was analyzed in real time by either a Fourier transform infrared spectrometer (FTIR, Tensor-27, Bruker, Ettlingen, Germany) or a quadrupole mass spectrometer (MS, QMS 403 D, Netzsch,

Germany), respectively. To prevent condensation of the emitted gas, the connecting tube between the TGA and FTIR or MS was maintained at 200 °C using a heating jacket. The FTIR spectrometer provided real-time distribution data for gaseous products, such as CO, CO_2, H_2O, and specific functional groups, such as C-C, C=C, and C=O. Meanwhile, the MS analyzer provided data for nitrogen-containing compounds. The FTIR spectrometer operates over a spectral range of 500 to 4000 cm^{-1}, achieving a resolution of 4 cm^{-1}. To prevent any secondary reactions, the sample cell is maintained at a constant temperature of 200 °C. For mass analysis, a spectrometer fitted with an electron-impact ion source operating at 70 eV was employed. Scanning of ion energies was carried out across the m/z range of 10–150, with a scan rate of 0.2 s per mass unit.

Moreover, the catalytic pyrolysis experiments of microalgae were conducted using a tubular reactor system comprising a quartz tube (Φ 50 mm × 800 mm), an electrical heating furnace (OTF-1200X, Kejing, Hefei, China), and a product collecting system. As for a typical catalytic pyrolysis test, a ceramic boat filled with a mixture consisting of catalyst and *Nannochloropsis* sp. in a weight ratio of 1:1 was placed at the end of the tubular reactor, which was purged by argon at a flow rate of 200 mL/min for 30 min to guarantee an inert atmosphere. Upon stabilizing the reactor at two typical RCLPy temperatures (450 °C and 600 °C), the ceramic boat was promptly pushed into the central region of the reactor. Simultaneously, liquid products were gathered using the quantitative isopropanol via an absorption bottle submerged in ice–water mixtures. Our previous experimental results [15] show a standard deviation below 5%, indicating good reproducibility of the proposed process. The collected liquid samples were then dehydrated with the absorbent anhydrous sodium sulfate, filtered through syringe filters, and subsequently analyzed by gas chromatography-mass spectrometry (GC–MS, 7890A-5975C, Agilent, Santa Clara, CA, USA). An HP-5MS capillary column was employed for the gas chromatography process. Compound identification was performed using the NIST 2017 library software.

4. Conclusions

In this study, the pyrolysis behavior of microalgae was systematically investigated using TG-FTIR, TG-MS analysis, and tubular-reactor experiments in the presence of both CaO and ZSM-5 catalysts. Key findings are as follows: (1) Gaussian fitting of DTG curves shows that CaO promotes lipid pyrolysis, while ZSM-5 enhances protein pyrolysis, therefore influencing oxygen and nitrogen migration in products. (2) Both catalysts remarkably reduce the nitrogen content in bio-oils; however, their mechanisms are different. CaO promotes the release of nitrogen as NH_3 and HCNO, while ZSM-5 may promote nitrogen conversion to undetected species such as N_2 or its retention within pyrolysis char. This leads to the content of nitrogen-containing compounds as low as 3.8 area%. (3) Both catalysts are capable of promoting the production of aromatics and aliphatic hydrocarbons, with their highest contents reaching up to 41.9 area% and 19.1 area%, respectively. (4) Both catalysts increase the oxygenated compound content but shift their types significantly. CaO promotes ketonization to form ketones, while ZSM-5 facilitates hydration to produce alcohols. These findings provide valuable insights for the design of bifunctional material for the microalgae RCLPy process, thereby contributing to improving bio-oil quality from microalgae biomass.

Supplementary Materials: The following supporting information can be downloaded at https://www.mdpi.com/article/10.3390/catal16020126/s1. Tables S1 and S2: GC-MS analysis results of pyrolysis oils without catalyst at 450 °C and 600 °C, respectively; Tables S3 and S4: GC-MS analysis results of pyrolysis oils with CaO as catalyst at 450 °C and 600 °C, respectively; Tables S5 and S6: GC-MS analysis results of pyrolysis oils with ZSM-5 as catalyst at 450 °C and 600 °C, respectively; Table S7: Summary of GC-MS analysis results of pyrolysis oils at different situations.

Author Contributions: Conceptualization, Y.L.; methodology, Y.L. and W.Z.; software, W.L. and X.K.; validation, W.Z., W.L. and X.K.; formal analysis, W.Z.; investigation, W.Z., X.K. and W.L.; resources, W.Z.; data curation, Y.L.; writing—original draft preparation, W.Z. and Y.L.; writing—review and editing, Y.L.; visualization, W.Z.; supervision, Y.L.; project administration, Y.L.; funding acquisition, Y.L. All authors have read and agreed to the published version of the manuscript.

Funding: This research was funded by the National Natural Science Foundation of China (Grant No. 22479084) and Shandong Provincial Natural Science Foundation (Grant No. ZR2025MS739).

Data Availability Statement: The original contributions presented in this study are included in the article. Further inquiries can be directed to the corresponding authors.

Conflicts of Interest: The authors declare no conflicts of interest.

References

1. Sarwer, A.; Hamed, S.M.; Osman, A.I.; Jamil, F.; Al-Muhtaseb, A.H.; Alhajeri, N.S.; Rooney, D.W. Algal biomass valorization for biofuel production and carbon sequestration: A review. *Environ. Chem. Lett.* **2022**, *20*, 2797–2851. [CrossRef]
2. Zuorro, A.; García-Martínez, J.B.; Barajas-Solano, A.F. The application of catalytic processes on the production of algae-based biofuels: A Review. *Catalysts* **2021**, *11*, 22. [CrossRef]
3. Widawati, T.F.; Pancasakti, B.P.; Kinanthi, D.H.; Sudibyo, H.; Marcos; Budiman, A. Unraveling the chemistry of microalgae pyrolysis: Connecting macromolecules to diverse high-value products. *Resour. Chem. Mater.* **2025**, 100150. [CrossRef]
4. Yang, C.; Li, R.; Zhang, B.; Qiu, Q.; Wang, B.; Yang, H.; Ding, Y.; Wang, C. Pyrolysis of microalgae: A critical review. *Fuel Process. Technol.* **2019**, *186*, 53–72. [CrossRef]
5. Li, F.H.; Srivatsa, S.C.; Bhattacharya, S. A review on catalytic pyrolysis of microalgae to high-quality bio-oil with low oxygeneous and nitrogenous compounds. *Renew. Sustain. Energy Rev.* **2019**, *108*, 481–497. [CrossRef]
6. Andrade, L.A.; Batista, F.R.X.; Lira, T.S.; Barrozo, M.A.S.; Vieira, L.G.M. Characterization and product formation during the catalytic and non-catalytic pyrolysis of the green microalgae Chlamydomonas reinhardtii. *Renew. Energy* **2018**, *119*, 731–740. [CrossRef]
7. Ilyin, S.O.; Makarova, V.V. Bio-Oil: Production, Modification, and Application. *Chem. Technol. Fuels Oils* **2022**, *58*, 29–44. [CrossRef]
8. Shirazi, Y.; Viamajala, S.; Varanasi, S. In-situ and ex-situ catalytic pyrolysis of microalgae and integration with pyrolytic fractionation. *Front. Chem.* **2020**, *8*, 786. [CrossRef] [PubMed]
9. Sardi, B.; Ningrum, R.F.; Ardiansyah, V.A.; Qadariyah, L.; Mahfud, M. Production of liquid biofuels from microalgae chlorella sp. via catalytic slow pyrolysis. *Int. J. Technol.* **2022**, *13*, 147–156. [CrossRef]
10. Zainan, N.H.; Srivatsa, S.C.; Bhattacharya, S. Catalytic pyrolysis of microalgae *Tetraselmis suecica* and characterization study using in situ synchrotron-based infrared microscopy. *Fuel* **2015**, *161*, 345–354. [CrossRef]
11. Chagas, B.M.E.; Dorado, C.; Serapiglia, M.J.; Mullen, C.A.; Boateng, A.A.; Melo, M.A.F.; Ataíde, C.H. Catalytic pyrolysis-GC/MS of Spirulina: Evaluation of a highly proteinaceous biomass source for production of fuels and chemicals. *Fuel* **2016**, *179*, 124–134. [CrossRef]
12. Xu, W.; Ding, K.; Hu, L. A mini review on pyrolysis of natural algae for bio-fuel and chemicals. *Processes* **2021**, *9*, 2042. [CrossRef]
13. Li, W.; Zhao, L.; Jiang, X.; Yu, Z.; Liu, Y. Reverse chemical looping pyrolysis characteristics of pine wood biomass over reduced $Ca_2Fe_2O_5$ oxygen carrier. *J. Anal. Appl. Pyrolysis* **2025**, *191*, 107177. [CrossRef]
14. Liu, Y.; Wang, T.; Zhang, X.; Hu, X.; Liu, T.; Guo, Q. Chemical looping staged conversion of microalgae with calcium ferrite as oxygen carrier: Pyrolysis and gasification characteristics. *J. Anal. Appl. Pyrolysis* **2021**, *156*, 105. [CrossRef]
15. Liu, Y.; Liu, J.; Wang, T.; Zhang, X.; Wang, L.; Hu, X.; Guo, Q. Co-production of upgraded bio-oil and H_2-rich gas from microalgae via chemical looping pyrolysis. *Int. J. Hydrogen Energy* **2021**, *46*, 24942–24955. [CrossRef]
16. Kang, H.; Guo, X.; An, M.; Guo, Q.; Chang, G. Preparation of aromatic hydrocarbons from pinecone pyrolysis synergistically catalyzed by Ca–Fe and HZSM-5. *J. Anal. Appl. Pyrolysis* **2023**, *172*, 106022. [CrossRef]
17. Zhang, X.; Sun, L.; Chen, L. Comparison of catalytic upgrading of biomass fast pyrolysis vapors over CaO and Fe(III)/CaO catalysts. *J. Anal. Appl. Pyrolysis* **2014**, *108*, 35–40. [CrossRef]
18. Sathish, T.; Saravanan, R.; Giri, J.; Al-Kahtani, A.A.; Prakash, C.; Kumar, A.; Angadi, V.J.; Wang, S.F.; Ubaidullah, M. Hydrogen conversion by microalgae through water gasification under different operating conditions, and Fe_2O_3, Al_2O_3, and CaO additives: An experimental study. *Int. J. Hydrogen Energy* **2025**, *104*, 289–301. [CrossRef]
19. Wang, Y.; Xing, Y.; Hong, C. Ca sorption/enhanced Fe-based oxygen carriers for chemical looping gasification of microalgae. *J. Environ. Chem. Eng.* **2025**, *13*, 116274. [CrossRef]
20. Razzak, S.A.; Khan, M.; Irfan, F.; Shah, M.A.; Nawaz, A.; Hossain, M.M. Catalytic co-pyrolysis and kinetic study of microalgae biomass with solid waste feedstock for sustainable biofuel production. *J. Anal. Appl. Pyrolysis* **2024**, *183*, 106755. [CrossRef]

21. Guo, Q.; Yang, L.; Wang, K.; Xu, X.F.; Wu, M.; Zhang, X.L. Effect of hydration-calcination CaO on the deoxygenation of bio-oil from pyrolysis of *Nannochloropsis* sp. *Int. J. Green Energy* **2019**, *16*, 1179–1188. [CrossRef]
22. de Deus Junior, J.O.; Alves, J.L.F.; Melo, V.R.D.E.; de Oliveira, A.A.S.; de Oliveira, K.F.S.; Melo, D.M.D.; Braga, R.M. Conversion of microalgae into renewable hydrocarbons through catalytic pyrolysis: A bibliometric analysis. *Algal Res.* **2024**, *81*, 103602. [CrossRef]
23. Zhou, Y.; Hu, C. Catalytic thermochemical conversion of algae and upgrading of algal oil for the production of high-grade liquid fuel: A review. *Catalysts* **2020**, *10*, 145. [CrossRef]
24. Thangalazhy-Gopakumar, S.; Adhikari, S.; Chattanathan, S.A.; Gupta, R.B. Catalytic pyrolysis of green algae for hydrocarbon production using HZSM-5 catalyst. *Bioresour. Technol.* **2012**, *118*, 150–157. [CrossRef] [PubMed]
25. Kumar, R.; Enjamuri, N.; Shah, S.; Al-Fatesh, A.S.; Bravo-Suárez, J.J.; Chowdhury, B. Ketonization of oxygenated hydrocarbons on metal oxide based catalysts. *Catal. Today* **2018**, *302*, 16–49. [CrossRef]
26. Chen, W.H.; Chu, Y.H.; Liu, J.L.; Chang, J.S. Thermal degradation of carbohydrates, proteins and lipids in microalgae analyzed by evolutionary computation. *Energy Convers. Manag.* **2018**, *160*, 209–219. [CrossRef]
27. Pham, T.N.; Sooknoi, T.; Crossley, S.P.; Resasco, D.E. Ketonization of carboxylic acids: Mechanisms, catalysts, and implications for biomass conversion. *ACS Catal.* **2013**, *3*, 2456–2473. [CrossRef]
28. Staš, M.; Kubička, D.; Chudoba, J.; Pospíšil, M. Overview of analytical methods used for chemical characterization of pyrolysis bio-oil. *Energy Fuels* **2014**, *28*, 385−402. [CrossRef]
29. Li, H.; Wang, Y.; Zhou, N.; Dai, L.; Deng, W.; Liu, C.; Cheng, Y.; Liu, Y.; Cobb, K.; Chen, P.; et al. Applications of calcium oxide-based catalysts in biomass pyrolysis/gasification-A review. *J. Clean. Prod.* **2021**, *291*, 125826. [CrossRef]
30. Meng, J.; Wang, J.; Yang, F.; Cheng, F. Study on the multiple roles of CaO on nitrogen evolution mechanism of protein inside sewage sludge pyrolysis. *Chem. Eng. J.* **2023**, *458*, 141039. [CrossRef]
31. Peng, J.; Li, J.; Zhong, D.; Zeng, K.; Xu, K.; Gao, J.; Nzihou, A.; Zhang, X.; Yang, H.; Chen, H. Transformation of nitrogen during solar pyrolysis of algae in molten salt. *Fuel Process. Technol.* **2023**, *242*, 107664. [CrossRef]
32. Chen, W.; Yang, H.; Chen, Y.; Xia, M.; Chen, X.; Chen, H. Transformation of nitrogen and evolution of N-containing species during algae pyrolysis. *Environ. Sci. Technol.* **2017**, *51*, 6570−6579. [CrossRef] [PubMed]
33. Yi, L.L.; Liu, H.; Lu, G.; Zhang, Q.; Wang, J.X.; Hu, H.Y.; Yao, H. Effect of mixed Fe/Ca additives on nitrogen transformation during protein and amino acid pyrolysis. *Energy Fuels* **2017**, *31*, 9484–9490. [CrossRef]
34. Tang, R.; Li, Y.; Yuan, Y.; Che, Y.; Gao, Y.; Shen, Z.; Zhang, J. Utilization of metal-functionalized ZSM-5 for methanol and low-carbon hydrocarbon coupling aromatization. *Processes* **2024**, *12*, 2724. [CrossRef]
35. Wang, S.; Shang, H.; Abomohra, A.E.-F.; Wang, Q. One-step conversion of microalgae to alcohols and esters through co-pyrolysis with biodiesel-derived glycerol. *Energy Convers. Manag.* **2019**, *198*, 111792. [CrossRef]
36. Hu, Y.; Wang, H.; Lakshmikandan, M.; Wang, S.; Wang, Q.; He, Z.; Abomohra, A.E.-F. Catalytic co-pyrolysis of seaweeds and cellulose using mixed ZSM-5 and MCM-41 for enhanced crude bio-oil production. *J. Therm. Anal. Calorim.* **2021**, *143*, 827–842. [CrossRef]
37. Li, W.; Zhao, L.; He, X.; Liu, J.; Liu, Y.; Guo, Q. Preparation of value-added chemicals via chemical looping pyrolysis of corn straws with Ca-Fe composite Oxygen carrier. *Fine Chem. Eng.* **2024**, *5*, 319–332. [CrossRef]

Disclaimer/Publisher's Note: The statements, opinions and data contained in all publications are solely those of the individual author(s) and contributor(s) and not of MDPI and/or the editor(s). MDPI and/or the editor(s) disclaim responsibility for any injury to people or property resulting from any ideas, methods, instructions or products referred to in the content.